1-1-2004

Noise Simulations For an Inverse-Geometry Volumetric CT System

Taly Gilat Schmidt
Marquette University, tal.gilat-schmidt@marquette.edu

Rebecca Fahrig
Stanford University

Norbert J. Pelc
Stanford University

Noise simulations for an inverse-geometry volumetric CT system

Taly Gilat Schmidt[a,b], Rebecca Fahrig[a], Norbert J. Pelc[a]

[a]Department of Radiology, Stanford University, Stanford, CA 94305
[b]Department of Electrical Engineering, Stanford University, Stanford, CA 94305

ABSTRACT

This paper examines the noise performance of an inverse-geometry volumetric CT (IGCT) scanner through simulations. The IGCT system uses a large area scanned source and a smaller array of detectors to rapidly acquire volumetric data with negligible cone-beam artifacts. The first investigation compares the photon efficiency of the IGCT geometry to a 2D parallel ray system. The second investigation models the photon output of the IGCT source and calculates the expected noise. For the photon efficiency investigation, the same total number of photons was modeled in an IGCT acquisition and a comparable multi-slice 2D parallel ray acquisition. For both cases noise projections were simulated and the central axial slice reconstructed. In the second study, to investigate the noise in an IGCT system, the expected x-ray photon flux was modeled and projections simulated through ellipsoid phantoms. All simulations were compared to theoretical predictions. The results of the photon efficiency simulations verify that the IGCT geometry is as efficient in photon utilization as a 2D parallel ray geometry. For a 10 cm diameter 4 cm thick ellipsoid water phantom and for reasonable system parameters, the calculated standard deviation was approximately 15 HU at the center of the ellipsoid. For the same size phantom with maximum attenuation equivalent to 30 cm of water, the calculated noise was approximately 131 HU. The theoretical noise predictions for these objects were 15 HU and 112 HU respectively. These results predict acceptable noise levels for a system with a 0.16 second scan time and 12 lp/cm isotropic resolution.

Keywords: computed tomography (CT), volume CT, image noise

1. INTRODUCTION

The development of multi-slice computed tomography (CT) detectors has enabled volumetric imaging with faster scan times, reduced motion artifacts, and thinner slices compared to single-slice scanners. This has also stimulated research on systems with very wide detectors in the slice direction. Such a "cone-beam" system would be able to image a volume in a single rotation. However, these systems have a fundamental limitation as a single circular scan cone-beam acquisition does not acquire a sufficient dataset for accurate reconstruction of a volume.[1] Approximate algorithms are available and generally used.[2] At small cone angles the resulting artifacts are negligible, but as the detector size in the slice direction increases, the artifacts become more severe.

We have proposed an inverse-geometry volumetric CT system (IGCT) to acquire a sufficient dataset for a 15 cm thick volume in one circular scan in one second or less.[3] The IGCT system uses a large area scanned anode x-ray source and a smaller detector array. In the transverse direction the sampling is fan-like, and in the axial direction the source and detector have the same axial extent thus avoiding cone-beam artifacts.

In this paper, we first give a brief description of the IGCT geometry and reconstruction algorithm followed by an overview of CT noise. We then examine two aspects of the IGCT noise performance through simulations. The first investigation studies the photon utilization efficiency of the IGCT system compared to a multi-slice 2D parallel ray acquisition. The second study predicts the noise in the IGCT images by modeling the x-ray photon flux based on currently available components. Only noise due to photon statistics is considered in these simulations. Other sources of noise, such as scatter and electronic noise, are not simulated.
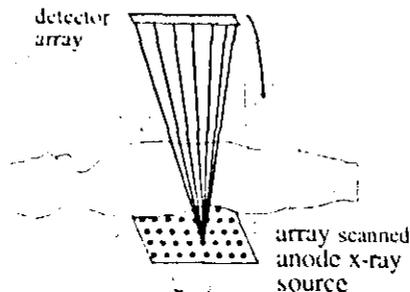
Figure 1. IGCT system with the x-ray beam at one collimator position.

2. METHODS AND MATERIALS

2.1. System Geometry

The basic system geometry is illustrated in Fig. 1. The proposed x-ray source has an electron beam that is electromagnetically steered across a transmission anode, dwelling at a series of source locations. An array of collimator holes limits the resulting x-ray beam at each location so that the beam illuminates only the detector. The detector is comprised of a smaller array of fast photon-counting detectors. The source and detector arrays are mounted on a gantry and rotated about the patient. For each source position, the entire detector array is read out producing a 2D divergent projection covering a fraction of the field of view (FOV). This is repeated for all source locations and for all gantry rotation angles. The scanning of the entire source is rapid compared to the gantry rotation.

The proposed source and detector arrays are conceptually similar to those used by NexRay Inc., for their cardiology C-arm system.[1]

2.2. Reconstruction Algorithm

The noise simulations described in this paper depend on accurate reconstruction of the IGCT data. The proposed reconstruction algorithm has been described previously,[3] however we will give a brief summary of the algorithm here.

In the IGCT system, the rays connecting each source row and the opposed detector row sample one transverse plane in the imaged volume. In the absence of noise, these in-plane rays ensure accurate reconstruction of the volume. In addition to these in-plane rays, there are also cross-plane rays which connect each source row to the remaining detector rows. This acquisition geometry is similar to that of a multi-ring PET system, therefore the proposed algorithm is based on a 3D PET reconstruction algorithm.[5,6] The data are first rebinned into 2D parallel-ray projections which are at multiple tilt angles to the axis of rotation. The output volume is then reconstructed using 3D filtered backprojection.

2.3. CT Noise

The variance, σ^2, in a reconstructed CT voxel depends on the total number of detected photons that passed through the voxel and the spatial resolution as expressed in the following equation,[7]

$$\sigma^2 = A \cdot \sum_{j=1}^{m} \frac{1}{N_j} \tag{1}$$

where N_j is the mean detected photon density that has passed through the voxel in the jth projection, and A is the integral of the reconstruction filter squared. For the specific case of multi-slice 2D parallel ray reconstruction

Further author information: (Send correspondence to T.G.S. E-mail: tgilat@stanford.edu)

(i.e., only the in-plane rays), A can be expressed as

$$A = \frac{\pi^2}{m^2} \int_{-\infty}^{\infty} \int_{-\infty}^{\infty} k_u^2 |W(\sqrt{k_u^2 + k_v^2})|^2 dk_u dk_v \tag{2}$$

where m is the number of projections, k_u and k_v are the coordinates of the 2D Fourier transform of the projection, and W is the window function, in our case a Hanning window with frequency cutoff k_c,

$$W(k) = \frac{1}{2}(1 + \cos(\frac{\pi k}{k_c})) \sqcap (\frac{k}{2k_c}) \tag{3}$$

Combining Eqs. 1, 2 and 3, and assuming that the photon density is the same for all projections, the relationship between the noise variance and the photon density, N, is

$$\sigma^2 = \frac{\pi^2 \int_{-\infty}^{\infty} \int_{-\infty}^{\infty} k_u^2 |W(\sqrt{k_u^2 + k_v^2})|^2 dk_u dk_v}{mN} \tag{4}$$

This expression will be used to verify the results of the noise simulations.

2.4. Photon Utilization Efficiency

The IGCT system uses ray measurements that cross transverse planes. The goal of this part of the study was to see if these rays introduce any noise penalty. To study this potential effect, we used the metric of photon utilization efficiency and modeled the same total number of photons in an IGCT acquisition and a multi-slice 2D parallel ray acquisition. Here we define the multi-slice 2D parallel ray geometry to consist of only in-plane rays and to have sampling and resolution comparable to the IGCT system.

For these simulations, the photon density was calculated such that the noise predicted by Eq. 4 would give a standard deviation of 10 HU in the slice reconstructed by the 2D parallel ray acquisition. From the photon density, which is defined as the number of photons per unit area, the total number of photons in the parallel ray acquisition can be calculated by

$$P_{total} = N \cdot pix_u \cdot pix_v \cdot area_d \cdot m \tag{5}$$

where pix_u and pix_v are the detector dimensions in pixels, and $area_d$ is the area of a detector element.

The total number of photons as calculated in Eq. 5 was distributed across all the rays in the IGCT geometry and noise projections simulated. For verification, multi-slice 2D parallel ray noise projections were also simulated with the same total number of photons. The parallel ray dataset was reconstructed with standard filtered backprojection. The IGCT data was rebinned into parallel ray projections and reconstructed as described in Section 2.2. For both cases the central axial slice was reconstructed and noise standard deviation measured across the slice.

2.5. Expected Noise

The photon efficiency simulation provides an estimate of the IGCT noise performance assuming a reasonable source output. In order to predict the expected noise of the IGCT reconstructions in a realistic system, we model the photon flux of the source based on currently available components, and simulate noisy data of ellipsoid phantoms. For simplicity, we assume monoenergetic photons.

We define the photon flux, F, to be the number of photons per second per mA per steradian. The number of photons in each IGCT ray measurement, P_{igct}, depends on the flux and can be calculated as

$$P_{igct} = F \cdot \frac{t \cdot area_d \cdot mA}{4\pi SDD^2} \tag{6}$$

where t is the dwell time at each source location, $area_d$ is the area of a detector element, and SDD is the source to detector distance.

Table 1. Specifications for simulated IGCT geometry.

Source dimensions (transverse x axial)	25 x 5 cm
Number of source locations	100 x 20
Detector dimensions (transverse x axial)	4.8 x 4.8 cm
Number of detector elements	48 x 48
Dwell time per source location	1 μs
Move time between successive source locations	0.28 μs
Source power	72 kW
Source voltage	120 kVp
Source to isocenter distance (SID)	41 cm
SDD	95 cm
FOV (transverse x axial)	10 cm x 5 cm

Using P_{igct} incident photons per ray measurement, noisy data was simulated for an ellipsoid water phantom ($\mu = 0.2$ cm^{-1}) located at the isocenter with diameters 10 cm by 10 cm by 4 cm. A second simulation was performed with the same size phantom with an attenuation coefficient of 0.6 cm^{-1}, that is with maximum attenuation equivalent to 30 cm of water. The central axial slice of each ellipsoid was reconstructed and the standard deviation measured for a small region of interest (ROI) at the center of the reconstructed slice.

For verification, a theoretical noise prediction was calculated for a multi-slice 2D parallel ray acquisition of the same phantoms using the same total number of photons. Eq. 4 was used for this calculation, with the photon density N calculated to be the density of detected photons exiting the center of the ellipsoid.

2.6. Simulation Details

The specifications of the simulated IGCT system are summarized in Table 1. These specifications are based on the current NexRay components, with possible modifications for comparison with a conventional CT geometry. For example, the NexRay system has a SDD of 150 cm and operates at a magnification of roughly three, while the investigated IGCT system has a SDD of 95 cm and operates at a magnification of roughly two. In the IGCT system the source focal spot size has been increased to 0.6 mm instead of the current 0.3 mm spot, which subsequently increases the possible source power.

Ideally, the source and detector areas would support a 30 cm by 15 cm FOV. However, since the initial investigations are based on currently available components, the FOV is limited to 10 cm by 5 cm.

For all simulations, 63 "views" over a 2π gantry rotation were simulated for the IGCT system, as this was the number necessary to sample Radon space sufficiently. A "view" is defined as all projections acquired by one scan of the source array and contains much more Radon space data than a single view in a conventional CT scanner. The IGCT data was rebinned into 2D parallel ray projections at 11 tilt angles ranging from -.03 to +.03 radians, with 1008 projections over 2π for each tilt angle. Each projection was 380 by 880 pixels, with a 1/8 mm by 1/8 mm pixel pitch.

The comparison multi-slice 2D parallel ray projections were also 380 by 880 pixels with a 1/8 mm by 1/8 mm pixel pitch and 1008 projections over 2π.

For all simulations, the reconstruction filter was apodized with a Hanning window with a cutoff of 15 lp/cm, unless otherwise noted. The 11.5 cm by 11.5 cm central axial slice was reconstructed, with a pixel pitch of 0.25 mm by 0.25 mm.

All simulations were repeated 10 times.

Table 2. Simulation results, with noise calculated as the standard deviation in Hounsfield units (HU)

Experiment	Theoretical noise	Theoretical noise (rebinning)	Simualted noise
Photon efficiency, 15 lp/cm cutoff	10	8.57	7.61 +/- 0.05
Photon efficiency, 7.5 lp/cm cutoff	10	9.61	9.44 +/- 0.13
Expected noise, μ=0.2 cm^{-1}	17.72	15.18	14.61 +/- 2.55
Expected noise, μ=0.6 cm^{-1}	130.96	112.18	131.23 +/- 24.50

3. RESULTS AND DISCUSSION

Simulation results are summarized in Table 2.

3.1. Photon Utilization Efficiency

Using Eq. 4 and the simulated geometry parameters, a total of $2.637 \cdot 10^{11}$ photons were determined necessary for a standard deviation of 10 HU in the parallel ray reconstruction. These photons were distributed to both the IGCT geometry and the parallel ray geometry. The calculated noise was 9.96 +/- 0.06 HU for the parallel ray simulations and 7.61 +/- 0.05 HU for the IGCT simulations, compared to the theoretical 10 HU.

The noise in the IGCT geometry is significantly lower than expected. This is most likely due to the blurring introduced during the rebinning step of the reconstruction algorithm. To verify this result, the same simulations were performed, but with the reconstruction filter windowed to a cutoff of 7.5 lp/cm for both systems. With the window width halved compared to the original simulation, the filter should dominate over the rebinning blur, and the IGCT system should have noise more comparable to the parallel ray system. The total number of photons was chosen using Eq. 4 to give a theoretical standard deviation of 10 HU. With these new parameters, the standard deviation of the simulated parallel ray reconstructions and IGCT reconstructions were 10.33 +/- 0.12 HU and 9.44 +/- 0.11 HU respectively.

Alternatively, the rebinning blur can be incorporated into the theoretical noise calculation. The majority of the rebinning blur can be accounted for by replacing Eq. 3 with the following expression which is derived in Appendix A.

$$\sigma^2 = \frac{\pi^2 \int_{-\infty}^{\infty} \int_{-\infty}^{\infty} k_u^2 |W(\sqrt{k_u^2 + k_v^2})|^2 |H(k_u)|^2 |H(k_v)|^2 dk_u dk_v}{mN} \tag{7}$$

where

$$H(k) = sinc(0.65k) + \frac{1}{2} sinc(0.65k - 1) + \frac{1}{2} sinc(0.65k + 1) \tag{8}$$

With $2.637 \cdot 10^{11}$ total photons and a filter cutoff of 15 lp/cm, Eqs. 7 and 8 predict a standard deviation of 8.57 HU, which is closer to the measured 7.61 HU.

The noise in the simulations is 5% to 10% lower than in a parallel beam system with the same photon density. This agreement is fairly good and suggests that using oblique rays does not introduce a penalty. The source of the residual disagreement is not known at this time.

3.2. Expected Noise

The flux of the NexRay source was calculated, through a combination of experimental measurement and Monte Carlo simulations, to be $3.164 \cdot 10^{13}$ photons/s/mA/sterad.[8]

Using Eq. 6 and assuming 1 mm^2 detector pixel area and the specifications in Table 1, the number of incident photons in each IGCT ray measurement is 2137 photons.

When this input flux was used to simulate IGCT data of a water ellipsoid with diameters 10 cm by 10 cm by 4 cm, the resulting noise at the center of the reconstructed slice, estimated with a 20 by 20 pixel ROI, was

14.61 +/- 2.55 HU. For a parallel ray acquisition with the same total number of photons, Eqs. 4 and 7 predict a noise level of 17.72 HU and 15.18 HU, without and with the rebinning blur respectively.

For the same ellipsoid phantom with attenuation equal to 0.6 cm^{-1}, the simulated standard deviation was 131.22 HU +/- 24.5 HU, compared to a predicted value of 130.96 HU without rebinning blurring and 112.18 HU with rebinning blurring.

Fig. 2 shows the reconstructed noise images for both ellipsoid phantoms.
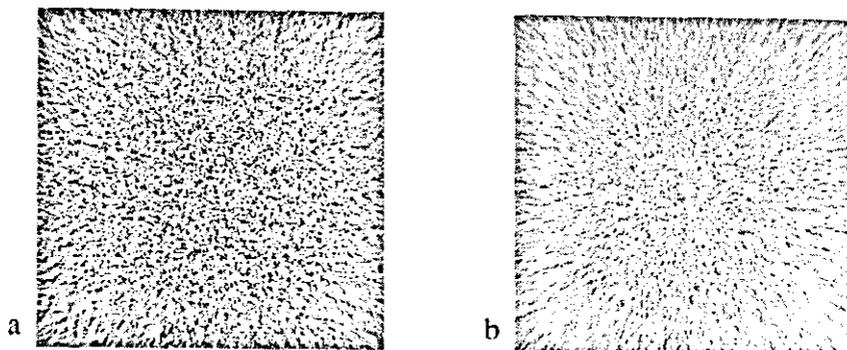
Figure 2. Reconstructed noise images. a) The central axial slice of an ellipsoid water phantom with diameters 10 cm by 10 cm by 4 cm, windowed to values between -1050 (black) and -950 HU (white). b) The central axial slice of the same phantom with $\mu = 0.6$ cm^{-1}, windowed to -1500 HU (black) and -500 (white).

3.3. Discussion

The simulation results suggest that the IGCT geometry is as efficient in photon utilization as a multi-slice 2D parallel ray geometry. That is, there is no noise penalty in using the IGCT system.

The predicted noise levels are encouraging and support further investigation of the IGCT system. We briefly analyze the differences between the simulated IGCT sytem and a conventional system as they relate to the expected noise.

The results presented in this paper pertain to a system with a relatively small FOV. In order to increase the FOV in the transverse direction, additional transverse source spots are required. To increase the axial FOV, additional axial source spots and detector elements are required. Because the sampling of the source and detectors within the FOV would not change significantly, we expect the photon efficiency results to be applicable to similar IGCT geometries with larger FOVs.

Increasing the FOV would, however, impact the scan time. For the simulated 10 cm by 5 cm FOV and the timing parameters in Table 1, each scan of the source is 2.56 ms. Therefore, a full acquisition (63 views over 2 π) takes 0.161 seconds. The detector read out time is faster than the time needed to steer the x-ray beam and is neglected in these calculations. If the FOV is increased by enlarging the source and detector areas, the scan time will scale with the total number of source spots. For example using a source with 200 by 60 spots (and a 5 cm by 15 cm detector) would produce a 30 cm by 15 cm FOV with a total scan time of 0.968 s. New IGCT geometries are being investigated which increase the transverse FOV by using multiple detector arrays, and thus do not increase the scan time.[9]

The IGCT system as described in this paper has an isotropic resolution of roughly 12 lp/cm., which is higher than that used when noise measurements are made on conventional scanners. This should be taken into account when evaluating the results of the ellipsoid phantom simulations, as the noise variance in CT is proportional to resolution to the fourth power.[7] Typical isotropic resolutions for a conventional CT scanner in high resolution mode is 8 lp/cm. The results in this paper predict a 54 HU standard deviation for a 30 cm water phantom for an IGCT acquisition with 8 lp/cm isotropic resolution.

Table 3. A comparison of noise measurements from a GE CT/I scanner and predicted noise for the IGCT system for a 48.5 cm polyethylene phantom, 0.625 mm in-plane resolution, one mm slice thickness, and one second total scan time.

	mAs	Noise (HU)
GE CT/I	200	56.5
IGCT	209	53.6

Table 3 summarizes the noise measured on a General Electric (GE) CT/I single slice scanner for a 48.5 cm polyethylene phantom at a one mm slice thickness. For comparison, the noise is predicted for the IGCT system for the same maximum attenuation and resolution. The effective mAs is calculated for the IGCT system based on the fraction of time that a voxel in the object is irradiated during a scan. That is, a voxel in the object only receives photons when the source is in certain array positions and does not receive photons while the beam is being steered. The effective mAs calculation also takes into account the increased efficiency of the transmission target used in the IGCT system.[4] As shown in Table 3, the predicted IGCT noise is comparable to the measured noise, and even slightly lower. The discrepency may be caused by noise sources not modeled in the IGCT calculation.

4. CONCLUSIONS

This paper examined the noise performance of an IGCT system. The results of the photon efficiency simulations verify that the IGCT geometry has comparable photon utilization efficiency to a 2D parallel ray geometry. The simulations predict acceptable noise levels for the fast scan time and high resolution. For example, for a 30 cm by 30 cm by 15 cm ellipsoid water phantom, 12 lp/cm isotropic resolution, and an effective mAs of 70 mAs, the expected noise standard deviation is 131 HU. Experiments with a table top system are planned to verify these theoretical results.

APPENDIX A. EXPECTED NOISE WITH REBINNING BLUR

The rebinning of the IGCT data into 2D parallel ray projections at multiple tilt angles is done by "gridding" which essentially convolves the data with a gridding kernel, and resamples the data onto a uniform grid.[10] The gridding is performed in a 4D Radon space, where the four dimensions are the rotation angle, tilt angle, and two distances which describe the location of each ray with respect to the central ray.

In our implementation, the 4D gridding kernel is defined as four separable 1D Hanning filters in each of the four dimensions. In the spatial domain, each kernel can be expressed as

$$h(x) = \frac{1}{w}(1 + \cos(\frac{2\pi x}{w})) \sqcap (\frac{x}{w}) \tag{9}$$

where w is the full kernel width, and the kernel has been normalized to have an area of 1.

The Fourier transform of this kernel is

$$H(k) = sinc(wk) + \frac{1}{2}sinc(wk - 1) + \frac{1}{2}sinc(wk + 1) \tag{10}$$

Since the convolution in Radon space is performed separately in each of the four dimensions, the corresponding filtering in frequency space can also be considered separately.

The two distance dimensions of the 4D Radon space are the same dimensions that are filtered when a 2D projection is filtered and backprojected. Therefore, the blur caused by gridding in these two dimensions can be modeled as part of the reconstruction filter. The modified reconstruction filter, $R(k)$ is

$$R(k) = \frac{\pi}{m}|k_u|W(\sqrt{k_u^2 + k_v^2})H(k_u)H(k_v) \tag{11}$$

and the modified noise relationship is

$$\sigma^2 = \frac{\pi^2 \int_{-\infty}^{\infty} \int_{-\infty}^{\infty} k_u^2 |W(\sqrt{k_u^2 + k_v^2})|^2 |H(k_u)|^2 |H(k_v)|^2 dk_u dk_v}{mN} \tag{12}$$

Eq. 12 can be used in place of Eq. 4 to calculate the expected noise of the IGCT system. The residual blurring in the two angular dimensions cannot be modeled in the reconstruction filter but should not affect the noise near the center of the image.

The gridding kernel width, w, used in these simulations was 0.65 mm.

ACKNOWLEDGMENTS

REFERENCES

1. B. D. Smith, "Cone-beam tomography: recent advances and a tutorial review," *Optical Engineering* **29**, pp. 524-534, 1990.
2. L. A. Feldkamp, L. C. Davis, and J. W. Kress, "Practical cone-beam algorithm," *J. Opt. Soc. Am.* **1**, pp. 612-619, 1984.
3. T. Gilat, R. Fahrig, and N. J. Pelc, "Three-dimensional reconstruction algorithm for a reverse geometry volumetric CT system with a large array scanned source," in *Medical Imaging 2003: Physics of Medical Imaging*. **5030**, pp. 103-111, SPIE, 2003.
4. E. G. Solomon, B. P. Wilfley, M. S. V. Lysel, A. W. Joseph, and J. A. Heanue, "Scanning-beam digital x-ray (SBDX) system for cardiac angiography," in *Medical Imaging 1999: Physics of Medical Imaging*, **3659**, pp. 246-257, SPIE, 1999.
5. M. Defrise, D. W. Townsend, and R. Clack, "Three-dimensional image reconstruction from complete projections," *Phys. Med. Biol.* **34**(5), pp. 573-587, 1989.
6. N. J. Pelc, *A generalized filtered backprojection algorithm for three dimensional reconstruction*. PhD thesis, Harvard University, 1979.
7. D. A. Chesler, S. J. Riederer, and N. J. Pelc, "Noise due to photon counting statistics in computed x-ray tomography," *J. Comput. Assist. Tomogr.* **1**, pp. 64-74, 1977.
8. J. Star-Lack. Personal communication.
9. S. Mazin, T. G. Schmidt, E. G. Solomon, R. Fahrig, and N. J. Pelc, "Geometry analysis of an inverse-geometry volumetric CT system with multiple detector arrays," in *Medical Imaging 2004: Physics of Medical Imaging*. **5368**, SPIE, 2004.
10. J. O'Sullivan, "A fast sinc function gridding algorithm for Fourier inversion in computer tomography," *IEEE Trans. Med. Imaging* **4**, pp. 200-207, 1985.